ISSN 1990-3413, Astrophysical Bulletin, 2014, Vol. 69, No. 2, pp. 121–140. © Pleiades Publishing, Ltd., 2014.
Original Russian Text © I.Yu. Katkov, O.K. Sil'chenko, V.L. Afanasiev, 2014, published in Astrofizicheskij Byulleten, 2014, Vol. 69, No. 2, pp. 129–149.

Properties of Stellar Populations in Isolated Lenticular Galaxies

I. Yu. Katkov[1,2*], O. K. Sil'chenko[1], and V. L. Afanasiev[3]

[1]*Sternberg State Astronomical Institute, Moscow State University, Moscow, 119992 Russia*

[2]*Physics Department, Lomonosov Moscow State University, Moscow, 119991 Russia*

[3]*Special Astrophysical Observatory, Russian Academy of Sciences, Nizhnii Arkhyz, 369167 Russia*

Received December 12, 2013; in final form, March 24, 2014

Abstract—We present the results of observations of a sample of isolated lenticular galaxies, performed at the SCORPIO and SCORPIO-2 spectrographs of the 6-meter BTA telescope of the SAO RAS in the long-slit mode. By direct spectra approximation, using the evolutionary synthesis models, we have measured the radial profiles of the rotation velocity as well as the dispersions of velocities, average age, and average metallicity of stars in 12 objects. The resulting average ages of the stellar population in bulges and discs fill an entire range of possible values from 1.5 to 15 Gyr which indicates the absence in the isolated lenticular galaxies, unlike in the members of groups and clusters, of a certain epoch when the structural components are formed: they could have been formed at a redshift of $z > 2$ as well as only several billion years ago. Unlike the S0 galaxies in a more dense environment, isolated galaxies typically have the same age of stars in the bulges and discs. The lenses and rings of increased stellar brightness, identified from the photometry of 7 of 11 galaxies, do not significantly differ from the stellar discs by the properties of stellar populations and velocity dispersion of stars. We draw a conclusion that the final arrangement of the morphological type of a lenticular galaxy in complete isolation is critically dependent on the possible modes of accretion of the cold external gas.

DOI: 10.1134/S1990341314020011

Key words: *galaxies: elliptical and lenticular—galaxies: stellar population—galaxies: evolution*

1. INTRODUCTION

The problem of the scenarios of formation and evolution of galaxies is the key issue in modern extragalactic astronomy and observational cosmology. The galaxies are formed under the influence of a large number of physical factors, which are often insufficiently known by the theorists in detail. The main issue here is to identify the most important factors which are crucial during the formation and evolution of galaxies of the given morphological type.

The type of lenticular (S0) galaxies was proposed by Edwin Hubble as hypothetical in 1936 [1] in order to fill in the intermediate position between the elliptical and spiral galaxies. It was assumed that the objects of this type have large-scale stellar discs as observed in the spiral galaxies but do not have any noticeable star-forming regions and spiral pattern in the stellar discs. Their smooth reddish view and probably an old average age of stars makes them similar to the elliptical galaxies. An intermediate position of lenticular galaxies between the purely spheroidal stellar systems and spiral galaxies, in which the contribution of the bulge to the total luminosity monotonically decreases with the transition from early to late types (from left to right along the morphological Hubble sequence), gives rise to a natural assumption that the S0 galaxies should possess large bulges. However, the detailed surface photometry of the images of S0 galaxies has shown that the bulges in them can be both very large and tiny [2]. Stemming from these results, the old idea of Van den Bergh [3], stating that the lenticular galaxies should be forming a sequence parallel to the spiral galaxies in the Hubble diagram and the connection between the (close) position in the diagram of the S0 (a, b, c) and spiral galaxies of the corresponding subtypes is given by the "bulge/disc" luminosity ratio [4, 5], becomes increasingly popular. It would seem that such a turn in the understanding of the evolutionary sense of the Hubble sequence would only reinforce the conventional wisdom about the formation of lenticular galaxies via the cessation of star formation in spiral galaxies: the evolutionary stage of transformation of the progenitor galaxy to the resulting S0 galaxy is much easier to imagine when both galaxies have the same bulge/disc ratio. However, it should be noted that if the contribution of the bulge to the total luminosity in an S0 galaxy

*E-mail: katkov.ivan@gmail.com

is the same as in the spiral galaxy located nearby on the morphological diagram, then this leaves open the possibility of reverse transformation, the transformation of an S0 galaxy into a spiral which would have been quite impossible in the presence of a larger bulge in the S0 galaxy.

The literature discusses a considerable number of physical processes that could cease star formation in the disc of the spiral galaxy. Here are some of them:

(1) direct collisions of galaxies [6, 7];

(2) tidal effects from the dark halo of the cluster/group [8];

(3) "harassment," or the gravitational tidal influence of galaxies on each other at a sufficiently fast flyby [9];

(4) ram pressure of the hot intergalactic medium [10, 11];

(5) "starvation," or termination of star formation as a result of the disappearance of the external reserves of gas, previously maintaining the gas accretion onto the disc of the galaxy and feeding the processes of star formation [12].

These processes are closely related to the dense environment of galaxies, because only the clusters and rich groups of galaxies with their massive dark haloes can provide the necessary density of the hot intergalactic medium for the ram pressure and close mutual locations of galaxies for the appearance of tidal effects.

We know that lenticular galaxies are the dominant population of the nearby clusters of galaxies, where their fraction reaches up to 60% [13]. However, the number of S0 galaxies is quite noticeable among the field galaxies as well: according to the APM survey [14], the fraction of lenticular galaxies in the nearby Universe is about 15%, and they are the second by the frequency of occurrence after the spirals. Furthermore, there are examples of completely isolated lenticular galaxies [15]. There appears a question which has not yet been raised about the origin of such galaxies. Under the effect of which physical mechanisms they were formed, and how do these mechanisms differ from those that work in the dense environment?

Despite the apparent deficit of mechanisms responsible for the morphological transformation of isolated galaxies compared to the members of clusters and groups, it is wrong to assume that the isolated galaxies evolve completely independently, as in the "closed box" scenario. Some recent studies point at this. In our work [16] we have demonstrated that a completely isolated early-type spiral galaxy NGC 7217 over the last 5 Gyr experienced at least two events of companion merger. In a locally isolated S0 galaxy NGC 4124 we also found traces of minor merging, which had apparently occurred 2–3 Gyr ago and provoked a central burst of star formation [17]. Furthermore, it was recently found out that lenticular field galaxies often possess significant amounts of gas. Moreover, it is exactly in the rarefied environment that a galaxy often reveals different kinematics of stars and gas, pointing to the external origin of gas [18]. Thus, the studies of the properties of isolated lenticular galaxies would allow to concentrate on the evolutionary mechanisms, connected either with the internal disc instabilities or just the external accretion of gas and/or companions. It should be noted that the accretion of gas and/or minor merging events may not only cease the star formation in the disc but, on the contrary, provoke it [19, 20].

The objects presented in this paper are the nearby, strongly isolated lenticular galaxies, for which we have conducted the spectroscopic observations with the aim to determine the properties of their stellar populations as well as kinematics of stars and gas. The properties of ionized gas in the investigated objects are discussed in a separate paper [21], while in this paper we concentrate only on the properties of stellar populations.

The paper is structured as follows: Section 2 is devoted to the description of the selection of studied objects; the features of the spectral observations, reduction, and data analysis are discussed in Section 3; Section 4 presents the results on each galaxy; Sections 5 and 6 contain the discussion of the results and conclusions of the study.

2. SAMPLE SELECTION

We have compiled a sample of the nearby isolated lenticular galaxies using an approach that has recently been developed in the Laboratory of Extragalactic Astrophysics and Cosmology of the SAO RAS by Karachentsev, Makarov, and their coauthors. This approach was proposed and applied to the galaxies of the Local Supercluster and its surroundings with a view of their association into pairs [22], triplets [23], and groups [24], as well as for the identification of isolated galaxies [25]. The data on the radial velocities, apparent magnitudes, and morphological types of galaxies were taken from the updated HyperLeda database[1] and the NED database,[2] supplemented by the radial velocity measurements from the SDSS, 6dF, HIPASS, and

[1] http://leda.univ-lyon1.fr/

[2] http://ned.ipac.caltech.edu/

ALFALFA surveys. Clustering was carried out for the galaxies with the radial velocity relative to the Local Group of $V_{\rm LG} < 4000\,\mathrm{km\,s^{-1}}$ and galactic latitude of $|b| > 10°$. A peculiarity of the clustering algorithm proposed by the authors is to account for the individual characteristics of galaxies, specifically, the indicator of the galaxy mass—the K-band luminosity. Uniting the galaxies in systems pairwise, the authors suppose that each virtual pair has to satisfy the negative total energy condition and the condition of finding its components within the "zero velocity sphere," i.e., the galaxies of the pair do not recede from each other as a result of the Hubble expansion of space. The clustering algorithm involves an iterative revision of all galaxies of the original sample for their further integration of the bound pairs of galaxies that have common members in the groups or clusters. The details of the algorithm are given in the above papers. One of the intermediate products of the algorithm is a list of paired isolation indices between any two galaxies of the sample. The isolation index (II) of two galaxies is the value characterizing the dynamic mutual influence of both components on each other. In the case of an unbound pair, $\log II$ is positive and equal to the logarithm of the number of times by which it is necessary to increase the mass of one of the components so that the pair would meet the given association criteria. And conversely, in the case of a bound pair, $\log II$ is negative and equal to the logarithm of the number of times by which the mass has to be reduced to become unbound. The same value of the isolation index may be realized for a wide pair of galaxies of comparable luminosity and for a tight pair consisting of a giant galaxy and a nearby but faint companion.

The authors of this approach have kindly provided us the information about mutual isolation indexes for all galaxies of the Local Supercluster and its environs. Using this information, we have selected for our study the lenticular galaxies having $II > 2.5$ both for the galaxies of higher and lower luminosity as compared to the considered one.

We have conducted the spectroscopic observations of 12 galaxies from the resulting list in order to study the properties of stellar populations. Table 1 shows the five most influential neighbors of higher and lower luminosity for each studied galaxy as well as the information about the morphology, radial velocities, and absolute magnitudes. In the cases of the NGC 16 and NGC 3098 galaxies, the restrictions on the isolation from the potential companions of lower luminosities are not met. Both galaxies have a low-luminosity neighbor with $II = 1.9$, but due to a very large luminosity difference $\delta M_K \approx 5$ of values (the masses differ by about 100 times), we believe that the companions cannot have a significant gravitational effect on large galaxies, so these galaxies do not egress from the generally accepted selection criteria for isolated galaxies.

3. OBSERVATIONS AND DATA ANALYSIS

3.1. Observations

The observations of the sample of studied galaxies were carried out in the prime focus of the 6-m BTA telescope of the SAO RAS over the period of 2011–2012. The spectral data for all the galaxies, except NGC 6615 and NGC 6654, were obtained using the SCORPIO-2 focal reducer [26] in the long-slit mode with the slit size of $6' \times 1''$. In the observations we have used the VPHG 1200@540 holographic grating (the grism), which provides a spectral resolution of FWHM ≈ 4 Å in the operating range of 3800–7300 Å. This spectral range includes both the strong absorption lines, like Mg, Fe, G-band, and a number of emission lines (Hα, Hβ, [O III], [N II], etc.) that allows to explore both the kinematics, age, and chemical composition of the stellar component and the kinematics of ionized gas, and at the same time to diagnose the excitation mechanisms of ionized gas. The detector used was an E2V CCD 42-90 with the chip sized 2k$\times$4k which at the 1$\times$2 binning mode readout provides a spatial scale along the slit of $0''\!.357$ per pixel and dispersion of 0.86 Å per pixel. Unlike the other galaxies, NGC 6615 and NGC 6654 were observed in another instrumental configuration, namely, with the SCORPIO instrument [27] and the VPHG 2300G holographic grating that provided a spectral resolution of 2.2 Å in the range of 4800–5600 Å, and the use of the EEV CCD 42-40 detector with the chip sized 2k$\times$2k gave the same scale along the slit with the dispersion of 0.37 Å per pixel. During the observations the slit was oriented along the major axes of the galaxies. The log of observations (Table 2) gives the dates of observations, total exposures, average seeing during the exposure of each galaxy, and the position angle of the slit.

3.2. Initial Data Reduction

Initial data reduction was performed using the original programs, written in the IDL environment, and contained the following steps: accounting for the registration system bias by subtraction of the averaged zero exposure frame from all the images; accounting for the uneven illumination and inhomogeneities in the CCD sensitivity by the spectra of the flat-field calibration lamp; removal of the traces

Table 1. Table of the environment of the studied galaxies

Name	Morph. type		V_{sys}	M_K	Neighbors "from the top"				Neighbors "at the bottom"			
	HyperLeda	NED			Name	δM_K	δV	II	Name	δM_K	δV	II
					NGC 4814	1.034	278	31.0	PGC 046033	−3.949	−48	4.2
IC 0875	S0	S0	2913	−22.713	NGC 5218	1.175	−121	107.9	SDSSJ 1324...	−3.577	−126	10.3
					NGC 5322	2.242	993	126.9	NGC 4964	−0.851	268	57.3
					NGC 5430	1.491	−224	150.4	NGC 5109	−1.563	660	78.6
					UGC 08237	0.315	−86	179.2	SDSSJ 1259...	−4.268	−83	84.0
					IC 0356	1.793	1131	158.6	UGC 12247	−4.960	298	46.2
IC 1502	S0-a	$S0^{+}$	2237	−23.704	NGC 3031	−0.394	2135	280.1	UGC 12504	−4.322	−461	64.6
					NGC 1184	0.925	−264	311.8	UGC 12921	−2.427	−477	73.5
					IC 0342	−0.361	1997	376.8	UGC 12160	−1.135	404	74.2
					NGC 6951	1.074	517	473.3	UGC 12069	−2.052	−405	106.8
					NGC 7817	−0.190	745	214.2	PGC 000446	−5.443	−140	1.9
NGC 0016	E-S0	$SAB0^{-}$	3300	−24.511	NGC 0253	−0.100	3024	1029.7	UGC 12873	−5.043	−212	22.8
		edge-on			NGC 3031	−1.201	3198	1212.8	PGC 087206	−5.736	−513	191.4
					NGC 7619	1.071	−689	1296.4	PGC 001153	−6.733	−636	312.1
					NGC 7331	0.410	2179	1339.5	UGC 00285	−3.498	872	459.0
					NGC 2339	1.168	−396	135.1	UGC 03775	−4.638	−244	12.1
NGC 2350	S0-a	S0/a	1774	−22.725	NGC 2365	0.681	−429	400.0	UGC 03691	−0.708	−327	81.7
					NGC 3031	0.584	1672	402.6	PGC 097214	−2.601	−298	102.4
					NGC 4472	2.552	901	635.7	PGC 2807004	−5.452	40	172.1
					IC 0342	0.618	1534	1054.5	–	−5.371	−154	470.6

Table 1. (Contd.)

Name	Morph. type		$V_{\rm sys}$	M_K	Neighbors "from the top"				Neighbors "at the bottom"			
	HyperLeda	NED			Name	δM_K	δV	II	Name	δM_K	δV	II
NGC 3098	S0-a	S0 edge-on	1305	−22.170	NGC 3190	1.456	117	4.1	PGC 2806869	−4.981	58	1.9
					NGC 3245	1.216	29	27.1	IC 2520	−1.545	151	24.1
					NGC 3227	0.955	271	40.4	UGC 05588	−2.090	95	33.0
					NGC 2964	1.033	44	49.0	PGC 029347	−2.527	10	37.5
					NGC 3379	1.618	544	53.3	NGC 3026	−1.433	−109	38.5
NGC 3248	S0	S0	1356	−21.818	NGC 3190	1.808	168	2.5	PGC 166105	−5.029	252	13.2
					NGC 3301	0.782	116	6.3	PGC 2806870	−5.424	−115	16.0
					NGC 3245	1.568	80	15.9	PGC 030270	−3.603	−78	24.1
					NGC 3227	1.307	321	21.4	UGC 05588	−1.738	145	35.6
					NGC 3379	1.970	594	38.5	PGC 031387	−2.524	47	36.9
NGC 6615	S0-a	SB0$^+$?	2868	−23.779	NGC 6574	0.520	396	21.7	UGC 11214	−1.687	34	2.5
					UGC 11057	−0.299	−161	92.4	PGC 061685	−2.895	−198	2.9
					NGC 6548	0.244	498	110.9	PGC 061658	−1.804	−319	13.5
					NGC 6501	0.432	−224	123.7	UGC 11168	−0.981	381	22.4
					NGC 6587	0.390	−429	138.0	PGC 061621	−0.776	−274	29.4
NGC 6654	S0-a	(R′)SB0/a(s)	2204	−23.830	NGC 6643	−0.203	459	21.1	PGC 062387	−3.539	101	18.4
					NGC 6340	−0.651	757	189.7	NGC 6654A	−3.756	380	25.6
					NGC 6951	0.948	484	225.3	UGC 10892	−4.568	26	33.3
					NGC 3031	−0.520	2102	273.3	PGC 062173	−3.925	534	51.3
					NGC 6911	0.517	−576	470.4	UGC 11295	−4.629	−427	57.8

Table 1. (Contd.)

Name	Morph. type		$V_{\rm sys}$	M_K	Neighbors "from the top"				Neighbors "at the bottom"			
	HyperLeda	NED			Name	δM_K	δV	II	Name	δM_K	δV	II
					NGC 6764	−0.001	41	31.1	UGC 11457	−4.740	−10	6.1
NGC 6798	S0	S0	2741	−23.520	NGC 6824	1.934	−1091	232.1	NGC 6757	−0.813	75	36.9
					NGC 6703	1.045	90	344.4	UGC 11502	0.047	−335	112.3
					NGC 6829	0.376	−853	505.2	PGC 063313	0.604	−1241	193.8
					NGC 6946	0.083	2389	577.0	NGC 6796	−0.424	263	303.2
					NGC 0253	3.488	801	137.0	PGC 069415	−1.826	61	2.5
NGC 7351	S0	SAB0^0?	1077	−20.923	NGC 7727	3.637	−881	899.2	PGC 069224	−1.777	−7	3.4
					NGC 3031	2.387	975	1006.1	PGC 1028063	−3.405	23	11.9
					IC 1459	4.208	−599	1042.6	PGC 982181	−5.031	−37	169.8
					NGC 7507	3.518	−558	1163.6	PGC 069293	0.579	−809	626.0
					NGC 2712	0.334	−50	66.2	UGC 04659	−2.959	17	26.7
UGC 04551	S0	S0?	1794	−22.633	NGC 2768	1.827	328	69.3	PGC 023834	−3.120	−10	27.5
					NGC 2639	2.259	−1458	71.1	UGC 04543	−1.791	−189	58.5
					NGC 3031	0.677	1691	127.7	UGC 04648	−3.851	−138	93.2
					NGC 2681	0.009	1048	159.4	UGC 04922	−1.653	−228	168.9
					NGC 4472	3.567	909	88.7	NGC 5727	−2.425	206	42.1
UGC 09519	S0	S0?	1782	−21.710	NGC 5353	3.466	−457	131.0	PGC 2080256	−3.641	−196	69.1
					NGC 5611	0.804	−243	152.5	PGC 052694	−2.617	132	72.0
					NGC 5582	0.986	247	159.8	UGC 09597	−3.886	−30	123.5
					NGC 5194	2.284	1221	194.7	NGC 5798	−0.596	−88	127.6

of cosmic particles by using the `L.A.Cosmic` [28] algorithm, implementing the Laplacian filter for particle detection, and by addition of spectra; construction of a two-dimensional dispersion equation by the spectrum of the helium-neon-argon calibration lamp and the further linearization of spectra with the characteristic accuracy of 0.03–0.06 Å depending on the grating used; subtraction of the background spectrum of the night sky; conversion of the instrumental fluxes in the absolute ones using the spectra of spectrophotometric standard stars. During the observations in semi-darkness the night sky contribution is large enough and varies with time. In such cases we performed the night sky subtraction before the spectrum addition to fit the parameters of the procedure for each spectrum the best way possible. The final result of the primary data reduction were not only the spectra of the objects but also the frames of the error level that were calculated based on the Poisson photon statistics and readout noise and were transformed along with the images of the object spectra at each reduction stage.

In addition to the spectra of objects and spectrophotometric stellar standards, the spectra of dawn or twilight sky were also analyzed in the process of data reduction, which, in the essence, represent the solar spectrum convoluted with the instrumental profile of the spectrograph. Therefore, the analysis of the spectra of the dawn or twilight sky allows to determine the behavior of the instrumental profile of the spectrograph along the spectrograph slit and along the direction of dispersion. The former is important to subtract the contribution of the night sky, and the latter allows to accurately determine the parameters of the kinematics of galaxies. The spectra of the dawn sky were reduced in the same manner as the spectra of the objects. The reconstruction of the instrumental profile and its use in analyzing the galaxies are described in detail in the following Section 3.3.

Table 2. Log of observations

No.	Name	Date	Exposure, s	Seeing, arcsec	PA, deg
1	IC 875	Apr 23, 2012	2700	2.5	−30
2	IC 1502	Nov 19, 2011	2700	2.5	52
3	NGC 16	Nov 20, 2011	1800	2.0	16
4	NGC 2350	Dec 13, 2012	6000	1.6	−73
5	NGC 3098	Apr 18, 2012	5400	1.2	−90
6	NGC 3248	Apr 22, 2012	2700	3.0	−45
7	NGC 6615	Sep 19, 2012	7200	1.0	−15
8	NGC 6654	Sep 20, 2012	6600	1.3	0
9	NGC 6798	Nov 20, 2011	5400	2.5	−30
10	NGC 7351	Nov 19, 2011	3600	2.0	0
11	UGC 4551	Dec 12, 2012	8400	2.0	−67
12	UGC 9519	Apr 24, 2012	4500	2.0	−105

3.3. Subtraction of Night Sky Contribution

In the analysis of objects of low surface brightness, special attention should be given to the careful subtraction of the contribution of the night sky, underestimation of which may lead to the systematic errors in determining the parameters of stellar populations of the studied objects [29]. In this paper we determine the properties of stellar populations of the structural components of the galaxy, including the stellar discs of low surface brightness. Therefore, we believe it is necessary to describe in detail the procedure of the night sky spectrum subtraction.

We have previously proposed a refined technique for subtracting the spectrum of the night sky for the long-slit spectroscopy of the low surface brightness objects in case of strong variations of the instrumental profile along the slit [29]. In that procedure the sky model is constructed by recalculating the spectrum of the sky from the edge regions on the slit to the region containing the spectrum of the object, applying the deconvolution procedure to the reference spectrum. The spectrum of the dawn/twilight sky, which carries the data on the variations of the instrumental profile, is supposed to be used as a reference spectrum. Unfortunately, during the observations the spectra of the dawn/twilight sky were not always observed due to a sudden worsening of weather conditions. The standard method, which does not require the use of a reference spectrum and accounts in the zero approximation for the profile variations along the slit, consists in the approximation of the sky spectrum by the low-power polynomial (2–4) in each column of the spectrum image and its recomputation for the area of the object. This method works well for the spectra of non-extended objects. However, this condition is not always fulfilled in the long-slit observations of galaxies.

Therefore, we propose another way to build the spectrum of the night sky, which is based on the extrapolation procedure in the frequency domain. The spectrum of the night sky at a given position on the slit y–$S(\lambda, y)$ can be written as a convolution of the "true" spectrum of the night sky $S_0(\lambda)$ with the instrumental profile $\mathcal{L}(\lambda, y)$:

$$S(\lambda, y) = S_0(\lambda)\,\mathcal{L}(\lambda, y). \qquad (1)$$

In the frequency domain the convolution procedure becomes the multiplication procedure. Hence, if we perform a one-dimensional Fourier transform along the direction of dispersion, then

$$\mathrm{FFT}[S(\lambda, y)] = \mathrm{FFT}[S_0(\lambda)]\,\mathrm{FFT}[\mathcal{L}(\lambda, y)]. \quad (2)$$

As the analysis of the spectra of the dawn and twilight sky has shown, the shape of the instrumental profile of the SCORPIO/SCORPIO-2 spectrographs varies rather monotonously along the slit, therefore its Fourier transform $\mathrm{FFT}[\mathcal{L}(\lambda, y)]$ varies along the slit as monotonously. The first factor in the Fourier transform of the night sky spectrum is a constant function, hence in general the Fourier transform of the night sky along the slit varies monotonously. Using this fact and applying the standard polynomial extrapolation procedure to the spectrum of the night sky in the frequency domain, i.e., to its Fourier transform, and performing the subsequent inverse Fourier transform, we can construct the model of the spectrum of the night sky. The Fourier transform of the spectral image is a complex value, this is why the extrapolation should be performed separately for the real and imaginary parts of the Fourier transform. In this version of the model of the night sky, the reference spectrum of the dawn/twilight sky is not required. At the same time the quality of the model is comparable to the method based on the deconvolution procedure [29].

3.4. Data Analysis

Before the analysis of the spectra of galaxies, we analyzed the spectrum of the dawn sky in order to determine the variation of the parameters of the spectrograph instrumental profile (LSF—Line Spread Function) along and across the direction of dispersion which is required to correctly determine the internal kinematics of stars and gas in the galaxies. To do this, we have split the image of the dawn sky spectrum into many areas: 32 intervals along the slit and 7 segments along dispersion; in each section the dawn sky spectrum was summed to achieve the typical signal-to-noise relationship $S/N = 100$ per pixel. Next, we approximated the spectra from each area by the high-resolution solar spectrum, taken from the ELODIE 3.1 stellar spectral library [30], using the `ppxf` procedure of the per-pixel approximation of spectra [31]. In the approximation of the dawn sky spectrum, the instrumental profile has been parameterized by the Gauss–Hermite series of orthogonal functions [32]. As a result of approximation, we have obtained the instrumental profile parameters for different spectral regions. The mean characteristic width of the instrumental profile (in terms of velocity dispersion) for the observational mode with the VPHG 2300G and VPHG 1200@540 grating is $\sigma_{\mathrm{instr}} = 65\ \mathrm{km\,s^{-1}}$ and $\sigma_{\mathrm{instr}} = 90\ \mathrm{km\,s^{-1}}$ respectively.

The further analysis consisted of the approximation of the observed absorption spectra of galaxies by the high-resolution models of stellar population. To do this, we used the `NBursts` software package [33, 34], which is an extension of the `ppxf` per-pixel spectrum approximation method [31]. The applied approach allows to retrieve the information about the stellar component from all the available spectral regions simultaneously, in contrast to the analysis of the Lick indices of individual lines—the indicators of the properties of stellar populations. The approach of per-pixel approximation of the spectra of galaxies allows to easily exclude from the analysis the regions around the strong emission lines of ionized gas, it allows to avoid their systematic effect on the estimates of the stellar population parameters which is impossible when analyzing the Lick indices. Chilingarian et al. ([33, 34]) have shown that the per-pixel spectrum approximation method provides a 1.5–2 times higher accuracy of finding the stellar population parameters compared to the approach of the Lick indices.

The procedure of determining the parameters of the stellar population consists in the nonlinear minimization of the quadratic difference $\left(\chi^2\right)$ between the observed and model spectra. We have used synthetic spectra of stellar populations as model spectra. They were computed with the `Pegase.HR` [35] evolutionary code based on the ELODIE 3.1 high-resolution stellar spectral library [30] for the simple star formation history in the form of one short burst (SSP, Simple Stellar Population). The SSP stellar population model is set by the age of the star formation burst T (Gyr) and metallicity [Z/H] (dex), while the Salpeter initial mass function [36] is considered to be fixed in the model. To determine the stellar kinematics of the galaxy, the line-of-sight velocity distribution (LOSVD), which is given as the Gauss–Hermite quadrature [32], is entered in the model spectrum. Furthermore, the multiplicative continuum is included in the model which allows to consider the effect of the interstellar extinction on the shape of the spectrum of the galaxy as well as the errors of absolute calibration of the fluxes both in the observational data and in the stellar library, based on which the stellar population models were considered. To take into account the effect of the spectrograph on the spectrum of the galaxy, before the approximation of the observed spectra we convoluted the grid of stellar population models with the previously determined instrumental profile. The presence even of the weak emission lines and/or the residues from the subtraction of the strongest lines of the night sky can offset the stellar population parameter estimates. Hence, to eliminate

Table 3. Table of averaged parameters of the bulges, discs, lenses/rings

Galaxy	Averaging range, arcsec	Number of measurements	T, Gyr	[Z/H], dex	[Mg/Fe], dex	σ, km s^{-1}
			Bulge			
IC 875	4–7	10	$4.3^{\pm0.7}$	$-0.16^{\pm0.05}$	$0.20^{\pm0.04}$	$110^{\pm9}$
IC 1502	4–7	11	$17.6^{\pm0.9}$	$-0.04^{\pm0.06}$	$0.3^{\pm0.1}$	$168^{\pm16}$
NGC 16	2–5	10	$5.4^{\pm0.8}$	$-0.04^{\pm0.05}$	$0.19^{\pm0.04}$	$172^{\pm6}$
NGC 2350	4–7	8	$1.6^{\pm0.3}$	$-0.13^{\pm0.08}$	–	$103^{\pm15}$
NGC 3098	4–7	8	$5.4^{\pm0.4}$	$-0.10^{\pm0.02}$	$0.00^{\pm0.02}$	$73^{\pm6}$
NGC 3248	4–7	10	$4.8^{\pm0.6}$	$-0.11^{\pm0.05}$	$0.00^{\pm0.05}$	$77^{\pm5}$
NGC 6615	4–7	8	$10.8^{\pm1.5}$	$-0.26^{\pm0.05}$	$0.24^{\pm0.03}$	$129^{\pm5}$
NGC 6654	2–5	9	$12.2^{\pm1.4}$	$-0.19^{\pm0.07}$	$0.23^{\pm0.04}$	$158^{\pm5}$
NGC 6798	4–7	6	$8.0^{\pm1.9}$	$-0.20^{\pm0.05}$	$0.13^{\pm0.04}$	$115^{\pm7}$
NGC 7351	4–7	10	$2.2^{\pm0.5}$	$-0.37^{\pm0.08}$	$-0.03^{\pm0.06}$	$29^{\pm11}$
UGC 4551	4–7	8	$10.0^{\pm1.9}$	$-0.28^{\pm0.08}$	$0.15^{\pm0.03}$	$158^{\pm11}$
UGC 9519	4–7	9	$2.5^{\pm0.1}$	$-0.12^{\pm0.06}$	$0.04^{\pm0.03}$	$76^{\pm3}$
			Disc			
IC 875	13–45	16	$2.9^{\pm0.9}$	$-0.32^{\pm0.18}$	$0.26^{\pm0.07}$	$134^{\pm27}$
IC 1502	7–25	11	$16.7^{\pm1.6}$	$-0.13^{\pm0.10}$	$0.42^{\pm0.01}$	$130^{\pm25}$
NGC 16	6–30	18	$1.6^{\pm1.2}$	$-0.19^{\pm0.15}$	$0.16^{\pm0.02}$	$127^{\pm18}$
NGC 2350	10–40	15	$1.3^{\pm0.2}$	$-0.00^{\pm0.07}$	$0.06^{\pm0.07}$	$86^{\pm14}$
NGC 3098	25–60	18	$5.1^{\pm1.5}$	$-0.22^{\pm0.06}$	$0.08^{\pm0.02}$	$57^{\pm26}$
NGC 3248	10–39	31	$3.9^{\pm1.4}$	$-0.21^{\pm0.09}$	$-0.04^{\pm0.03}$	$65^{\pm17}$
NGC 6615	40–60	0	–	–	–	–
NGC 6654	35–60	3	$5.8^{\pm0.6}$	$-0.06^{\pm0.14}$	$0.40^{\pm0.20}$	$44^{\pm5}$
NGC 6798	8–55	18	$7.3^{\pm4.3}$	$-0.27^{\pm0.15}$	$0.11^{\pm0.12}$	$119^{\pm17}$
NGC 7351	17–45	7	$4.4^{\pm2.3}$	$-0.57^{\pm0.19}$	$-0.02^{\pm0.15}$	$72^{\pm40}$
UGC 4551	38–80	3	$10.9^{\pm4.3}$	$-0.74^{\pm0.39}$	$0.25^{\pm0.25}$	$107^{\pm20}$
UGC 9519	16–30	4	$2.9^{\pm0.9}$	$-0.32^{\pm0.17}$	$0.15^{\pm0.20}$	$98^{\pm15}$
			Lens/Ring			
IC 875	–	0	–	–	–	–
IC 1502	–	0	–	–	–	–
NGC 16	12–21	16	$3.3^{\pm2.9}$	$-0.25^{\pm0.16}$	–	$104^{\pm16}$
NGC 2350	20–26	1	$4.9^{\pm0.0}$	$-0.33^{\pm0.00}$	–	$97^{\pm0}$
NGC 3098	15–20	14	$4.8^{\pm1.3}$	$-0.13^{\pm0.05}$	$0.05^{\pm0.01}$	$57^{\pm12}$
NGC 3248	–	0	–	–	–	–
NGC 6615	20–40	3	$12.8^{\pm2.4}$	$-0.52^{\pm0.16}$	$0.21^{\pm0.06}$	$56^{\pm5}$
NGC 6654	–	0	–	–	–	–
NGC 6798	14–22	10	$5.2^{\pm2.1}$	$-0.30^{\pm0.14}$	$0.13^{\pm0.04}$	$97^{\pm15}$
NGC 7351	–	0	–	–	–	–
UGC 4551	17–35	12	$3.3^{\pm2.2}$	$-0.47^{\pm0.23}$	$0.23^{\pm0.03}$	$117^{\pm25}$
UGC 9519	7–15	22	$2.7^{\pm0.5}$	$-0.22^{\pm0.07}$	$0.05^{\pm0.02}$	$77^{\pm9}$

this effect, we have masked the regions sized 10–15 Å around them. As a result of the χ^2 minimization the following parameters are determined: the radial velocity v (km s^{-1}), the line-of-sight velocity dispersion σ (km s^{-1}), the estimates of age T (Gyr), and metallicity [Z/H] (dex) of the stellar population.

Spectroscopic observations were carried out with a long slit, which was oriented along the major axis of the studied galaxies. Since the surface brightness of galaxies greatly decreases with distance from the center, the spectra of the outer regions of the galaxy have a low S/N ratio. To increase it, we used the adaptive binning procedure, which consists in the summation of the spectrum in the intervals along the slit of variable size, set so that the S/N ratio is not less than the preassigned value (typically about 20–30) in each interval.

After subtracting the stellar component model from the observed spectrum of the galaxy, we got a purely emission spectrum of the galaxy. Every line was approximated by the Gaussians to obtain the line fluxes, velocities, and velocity dispersions of ionized gas. In this paper we only consider the properties of stellar populations, while [21] is dedicated to the study of the properties of ionized gas in the galaxies.

The `Pegase.HR` stellar population models were calculated based on the library of stars of the solar vicinity, possessing the solar α-element abundance. The resulting models are hence only computed for the solar abundance ratio. The methods for constructing the stellar population models are currently being developed taking into account non-solar α-element abundances (see, e.g., the studies [37] and [38]); however, the obtained models are calculated for a quite rare and limited grid of parameters and are so far inferior in quality to the models with the solar abundance of α-elements. The relative abundance of α-elements bears information on the duration of the star formation burst which has engendered the bulk of stars. If the burst was very short, shorter than 1 billion years, then the stellar population will be revealing an excess of α-elements with respect to iron in comparison with the solar chemical composition. Given a long history of star formation, the ratio of abundances of iron and α-elements, specifically magnesium, becomes solar [39, 40]. To estimate the abundance of α-elements in the stellar population of studied galaxies, in addition to the per-pixel approximation method we have applied to the spectra a more classical Lick index approach that allows to estimate the magnesium abundance (the α-process element). For the spectra of galaxies we have obtained the Lick Hβ, Mgb, Fe 5270, and Fe 5335 indices, determinations of which were taken from [41, 42]. A comparison of the obtained indices with the model values, calculated in the framework of stellar population synthesis models [43], allowed us to estimate the Mg/Fe ratio.

4. RESULTS

As a result of the spectral analysis, we have obtained for each studied galaxy the line-of-sight velocity profile of stars v, stellar velocity dispersion σ, and the properties of stellar populations: age T and metallicity [Z/H] (Fig. 1). In addition, we have analyzed the available photometric data for the considered galaxies and identified the areas where the disc begins to dominate, where the more complex morphological structures such as rings and lenses are present, and where in the center of the galaxy the region of the bulge dominance is present (where the nuclear region is excluded). For this, we used data from the public archive of the SDSS, DR9 survey, the r filter (for most galaxies), or, if the galaxies are not observed in the SDSS survey, we used the 2MASS survey data, the J, H, K filters (for NGC 2350, NGC 6798, IC 1502) and white-light images obtained at the SCORPIO-2 in the mapping mode before the spectral observations (NGC 6798, IC 1502). For the NGC 6798 and IC 1502 galaxies the image analysis results in the near infrared range and in the white light have coincided. For each galaxy we have conducted an isophote analysis and then treated the profiles of azimuthally averaged brightness. The outer regions well described by the exponential law of the surface brightness decay where constant ellipticity of the isophotes is noticeable were considered as the disc dominance regions. The local brightness excesses were sometimes visible in them, which we believe to be rings or lenses. To estimate the bulge parameters, we used a fixed range of radii, $4''$–$7''$. Over the regions isolated this way, we made the averaging of stellar population parameters with weights inversely proportional to the squares of individual estimate errors, $w_i = 1/\delta p_i^2$. The averaged parameter values for the bulges, discs, and rings or lenses are listed in Table 3. A graphical comparison of the derived parameters is demonstrated in Figs. 2, 3, and 4.

4.1. IC 875

In the HyperLeda and NED databases this galaxy is classified as lenticular S0, and hence it got to our sample. However, it proved to possess a sufficiently low rotation velocity. If we adopt the inclination as $i = 50°$ from the NED, then $V_{\rm rot} = \Delta V_{\rm LOS}/\sin i \approx 65$ km s^{-1} at the velocity dispersion of $\sigma \approx 110$ km s^{-1}, this gives the ratio of the rotation velocity to the velocity dispersion $V_{\max}/\sigma \approx 0.6$. The ratio of the large and small axes,

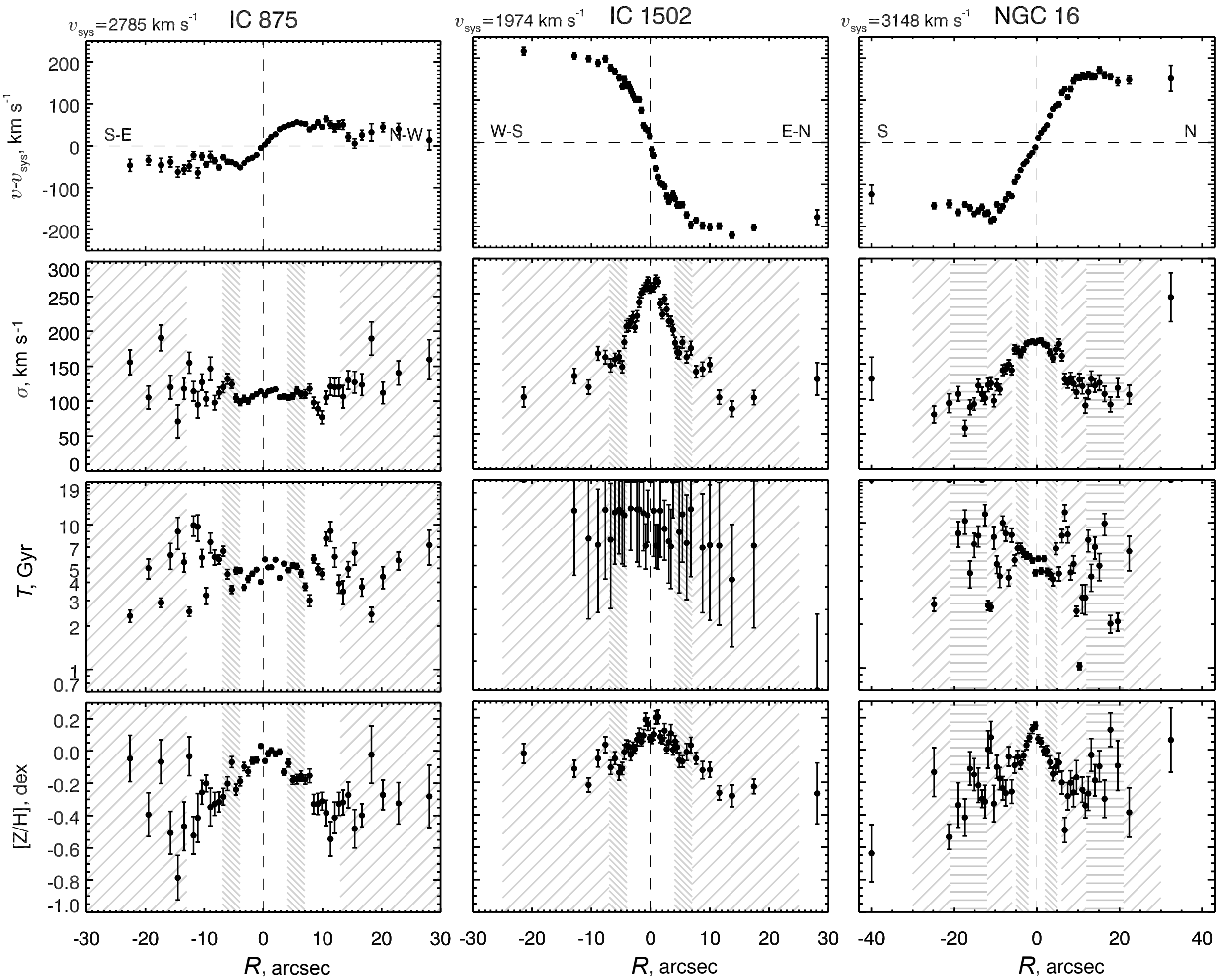

Fig. 1. The results of analysis of long-slit spectra of the studied galaxies. Each column corresponds to one galaxy. The panels with radial profiles of the line-of-sight velocity of stars net of the systematic velocity, velocity dispersions of stars, age, and metallicity are located from top to bottom. The distance from the center of the galaxy in arcseconds is plotted along the x-axis. The gray slashes mark the areas of the averaging of the bulge parameters (\) and the exponential disc parameters (/), the horizontal lines (—) are the regions of the lens or the ring, if present. The systematic velocity corresponds to the measured radial velocity of the galaxy's center, i.e., the brightest part, except for IC 875 where this is the center of symmetry of the central part of the velocity profile.

taken from NED, gives the ellipticity estimate of $\epsilon = 0.25$. These values fall in the diagram of Kormendy ($V_{\max}/\sigma$—ϵ) on the line of isotropic spheroids supported by rotation, which also contains elliptical low-luminosity galaxies [44]. IC 875 is probably an elliptical galaxy, we hence eliminated it from consideration, and it was not included in the construction of diagrams and distributions by the parameters for the isolated S0 galaxies.

4.2. IC 1502

According to the NED, this galaxy is classified as $S0^+$. It has a sufficiently large inclination $i = 64°$, according to the HyperLeda. The radial velocity profile indicates regular rotation. The main feature of this galaxy is that at the solar metallicity of stars the average age of stars is about 15—17 Gyr over the whole measured scope of the galaxy. The fact that this age is larger than the cosmological age of the Universe should not be confusing. The main components of the models are the isochrones of stars, which are the result of the stellar evolution theory and the empirical library of stellar spectra. It should be borne in mind that the stellar population models used do not contain the information about the cosmology of the Universe and give an absolutely independent channel of information about the age of the dominant stellar population in galaxies. The radial profiles of the parameters reveal the central kinematically detached region, which manifests itself as a slight increase

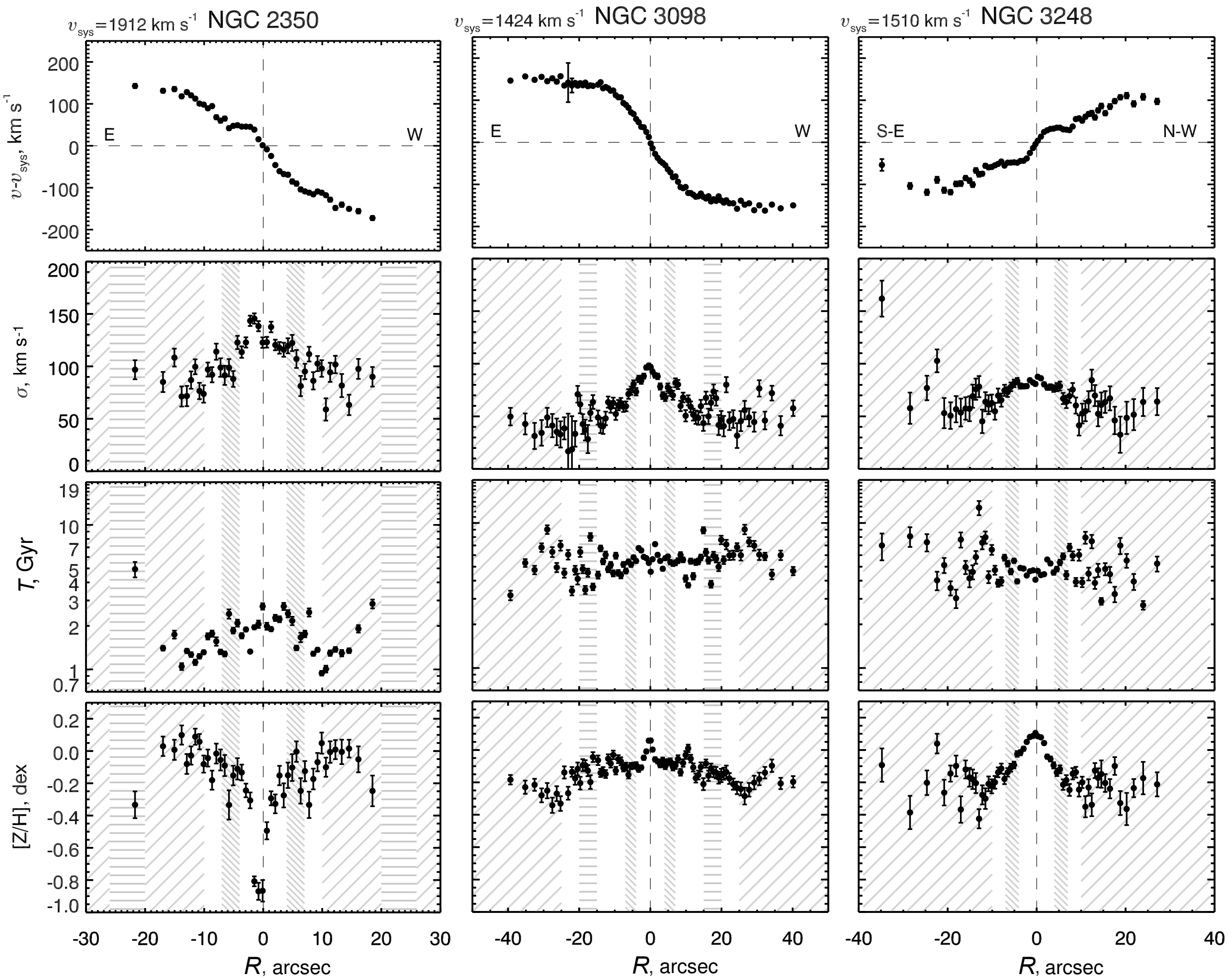

Fig. 1. (Contd.)

in the velocity gradient and a small decrease in the stellar velocity dispersion. The metallicity profile reveals a slight dip. This is probably the evidence of the evolutionary isolation of the nuclear star cluster, although by the age of stellar population it does not excel within the measurement error.

4.3. NGC 16

This galaxy has a small bar, oriented perpendicularly to the major axis of the galaxy, and a faint, $\Delta m_B = 4^{\rm m}$, late-type companion [45] 500 kpc from it. The isolation index between the companion and the galaxy is $II = 1.9$, but as the mass difference is about two orders of magnitude, we consider NGC 16 to be isolated from the external tidal effects. The galaxy has a very noticeable solid-body growth of the rotation curve of up to $10''$ from the center, where the rotation velocity goes on the plateau, and a dynamically hot enough disc, $\sigma > 100$ km s^{-1}. The stellar component has an intermediate age, while the bulge and the disc do not differ from each other in the mean, although individual age estimates in the bins have a sufficiently large scatter.

4.4. NGC 2350

This very poorly studied galaxy was unfortunately omitted by the field of view of the SDSS. According to the HyperLeda and NED, it is classified as S0/a. On the direct image obtained by the SCORPIO-2, we can see a complex distribution of stellar brightness in form of bright spots on the edges of the bar, the so-called "ansae" phenomenon. In addition, as we have found by analyzing the emission component of the spectrum, the galaxy has an extended disc of ionized gas. According to the location of the emission line ratios on the diagnostic diagrams, it was excited mainly by the radiation of young stars [21], i.e., this lenticular galaxy is currently undergoing the star formation across the entire disc. Correspondingly, the

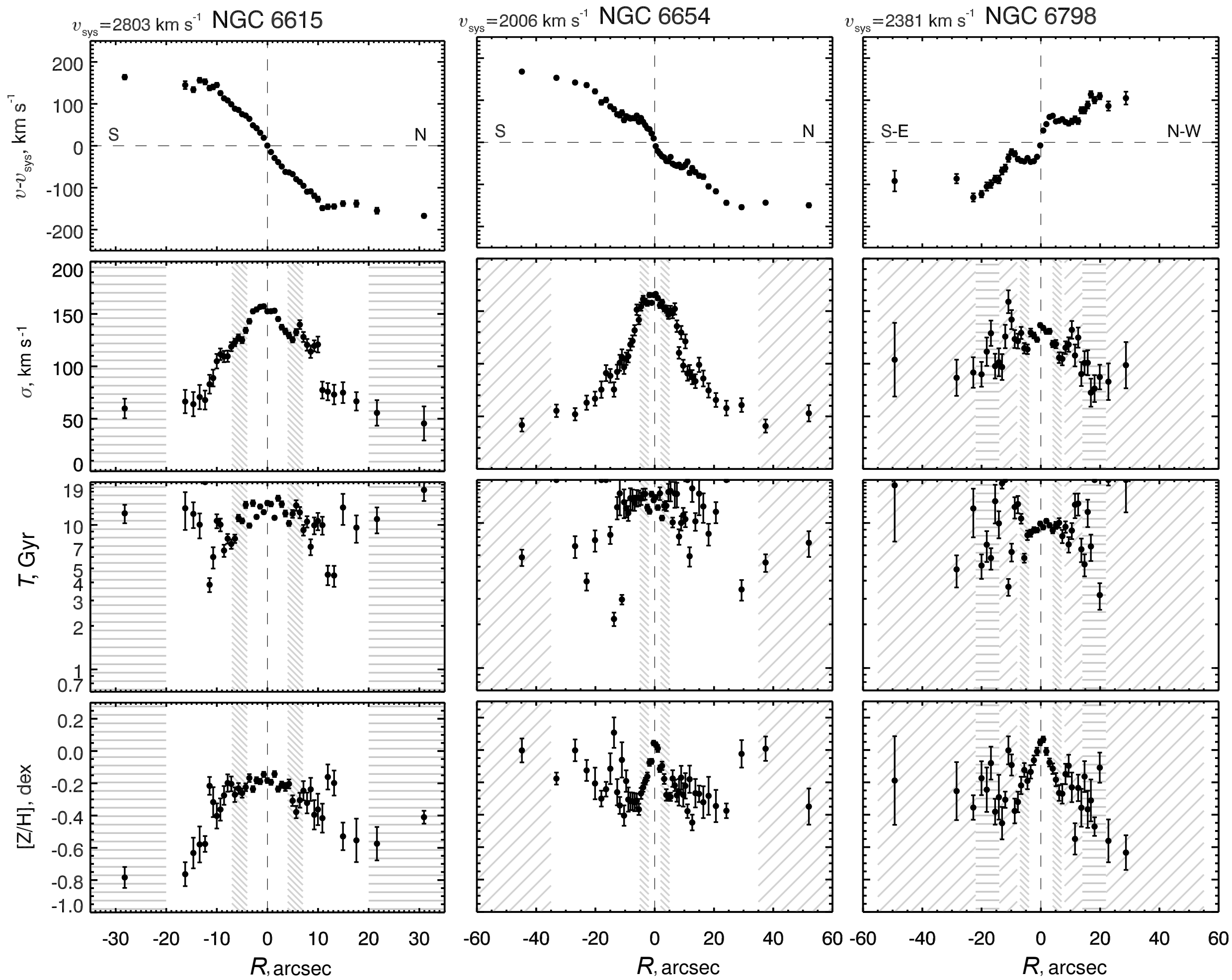

Fig. 1. (Contd.)

average age of stars within the area bordered by the "ansae" is pretty young: individual estimates in the bins are between 1 and 2 Gyr. In the central region of the galaxy the stars have a very low metallicity. This may be due to the earlier event of an infall on the galaxy of a metal-poor companion. At the same time this region is a little different in the rotation curve and the velocity dispersion distribution, but to our surprise it does not stand out in the age profile. According to our estimates, the metallicity of gas is weakly subsolar even in the region of a very low stellar metallicity. Therefore, the gas in this galaxy is probably not connected in its origins with a potentially possible merging, the traces of which are embodied in the nuclear stellar component.

4.5. NGC 3098

A very well-known isolated lenticular galaxy, oriented to the observer edge-on. Its photometric structure was studied in [46]. It was noted that the bulge of the galaxy is small and compact, and between the bulge and the disc, approximately at the radius of 15″, we observe a ring of enhanced stellar brightness. Our results (Fig. 1) confirm a small mass of the bulge—the rotation velocity growth in the center of the galaxy is quite hollow—and demonstrate a homogeneous age of the stellar population of 5–8 billion years across the galaxy as well as a sharp drop in metallicity of the stars in the transition from the central part of the galaxy to the region of dominance of the large-scale stellar disc. At that, the disc looks dynamically cold, $\sigma < 60$ km s^{-1}.

4.6. NGC 3248

Starting at a distance of 100 kpc, the galaxy is surrounded by a dozen of faint companions, the brightest of which is only 3^{m} fainter than the host galaxy. The central region of the galaxy, $R < 15''$, was investigated in detail by the panoramic spectroscopy at the

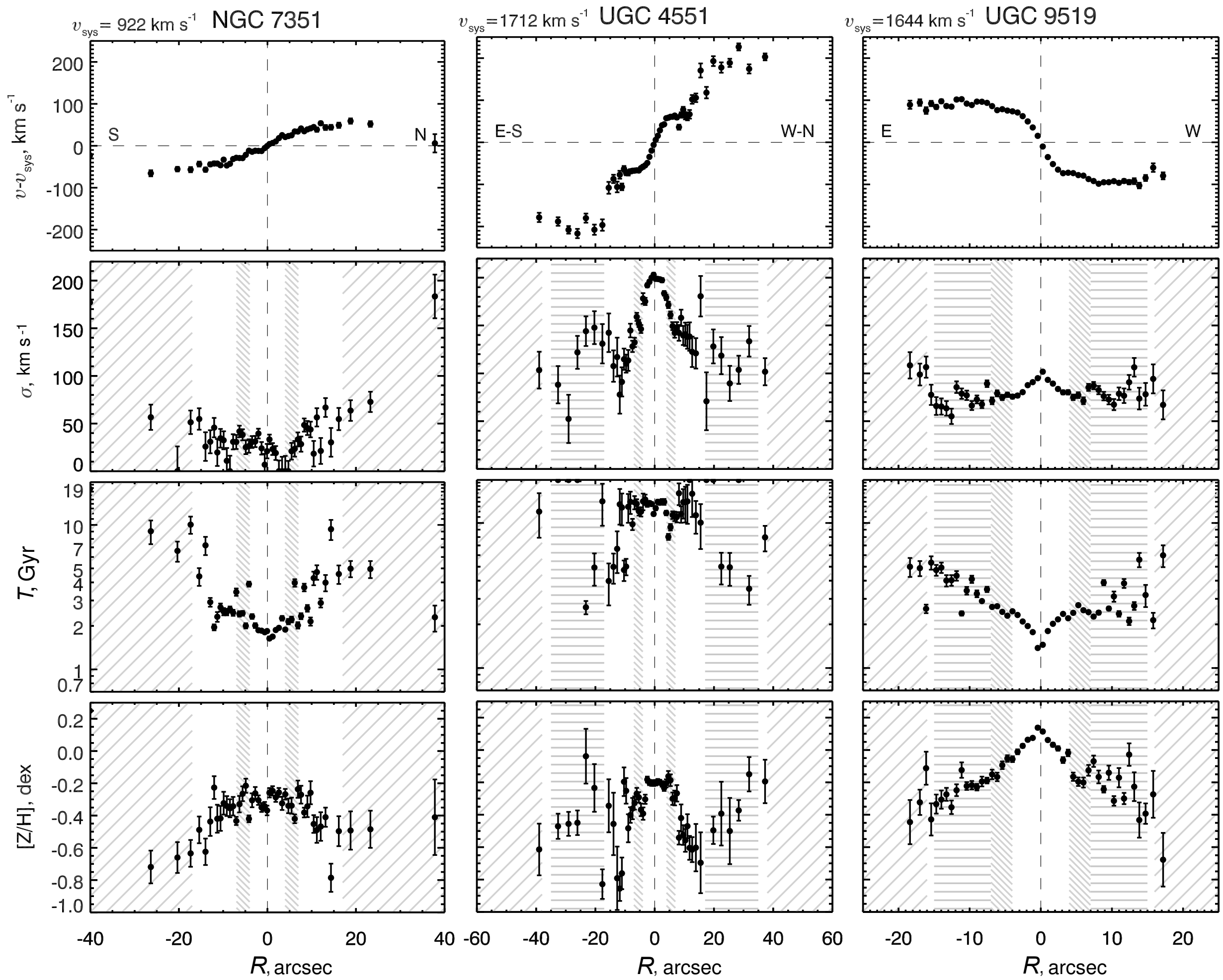

Fig. 1. (Contd.)

SAURON spectrograph within the ATLAS-3D survey [5, 18]. The galaxy proved to contain a lot of gas, both ionized and molecular, and this gas counter-rotates with respect to the stellar component. We have extended the kinematic profiles to the distance of 30″ from the center and confirmed the counter-rotation of gas concentrated in the central region of the galaxy. The gas excitation is shock-type, there are no signs of ongoing star formation. The age of the stellar population both in the center and in the galactic disc is intermediate, but the central regions are significantly more metal-rich than the disc.

4.7. NGC 6615

The galaxy is classified as barred in the databases. Visual analysis of the SDSS images confirms that a compact bar is present and oriented almost perpendicularly to the major axis of the galaxy. The surface brightness profile reveals a very noticeable extended lens with a flat brightness distribution, the exponential disc itself starts at the radii greater than 40″. The sensitivity of our spectroscopy with a high-resolution VPHG2300 holographic grating (the grism) was not enough to reach the disc, we have identified the characteristics of the stellar population only in the bulge and in the lens. The age of the stellar population is uniformly old throughout the entire measured part of the galaxy. It is possible that between bulge/bar and the lens a relatively younger narrow ring is present. The metallicity is below solar everywhere, while in the lens it is significantly lower than solar, at least 3–4 times. The gas in the galaxy has not been detected, but the lens is dynamically relatively cold.

4.8. NGC 6654

Quite a large galaxy with a large-scale bar and a disc of low surface brightness. The NED database classifies it as (R′)SB(s)0/a. We have borrowed the

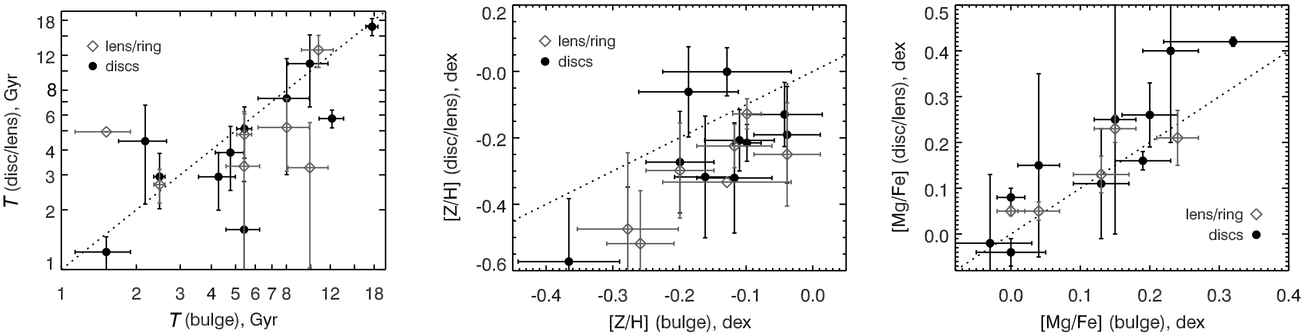

Fig. 2. A comparison of parameters of the stellar population in the bulges with the properties in discs and disc components: lenses/rings. The dashed line indicates the line of equal values.

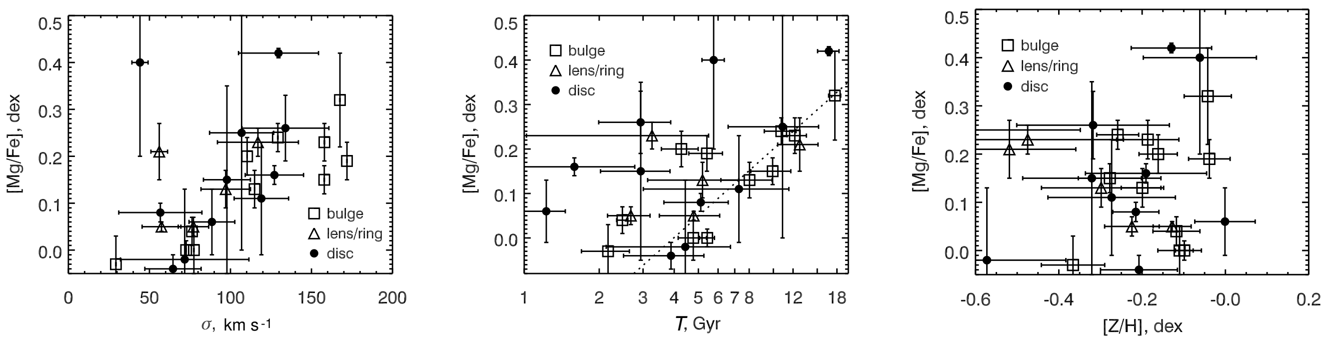

Fig. 3. A comparison of the velocities, age, and metallicity dispersion with relative enrichment of α elements ([Mg/Fe]) for different structural components of the galaxies.

analysis of the photometric structure of the galaxy from [2]. The outer edge of the disc reveals an emission gas ring of star formation. Apart from this outer ring, the gas is only present in the central region of the galaxy, where it demonstrates impact excitation and rotates too fast for the plane of symmetry of the galaxy, inclined at an angle of 45° to the line of sight (according to the HyperLeda). In our work [21] we have speculated that central gas rotates in the plane inclined to the main plane of symmetry of the galaxy. The characteristics of the stellar population (Fig. 1) indicate that the disc is younger and richer in metals than the bulge. Keeping in mind the residual star formation at the periphery of the disc, we can state that the NGC 6654 is a rare type of lenticular galaxies, where a rejuvenation (or secondary star formation) took place in the disc but not in the central region. Moreover, given the noticeable overabundance of magnesium relative to iron in the disc (Table 3), this rejuvenation had a character of a very brief burst in the expanding wave of star formation.

4.9. NGC 6798

Another galaxy after NGC 3248 which was investigated within the ATLAS-3D survey [5, 18] and in which a large-scale counter-rotating gaseous disc was found, while the neutral hydrogen in this galaxy continues to counter-rotate far beyond the stellar disc. Analyzing the photometric structure of the galaxy in the white-light image obtained with the SCORPIO-2, we noted the presence of a ring within $15''$–$20''$. This ring is aged 5 ± 2 Gyr which, accounting for the error bar, almost coincides with the age of the disc of 7 ± 4 Gyr . It is also slightly colder dynamically which is consistent with its possibly younger age. At the same time the metallicity of stars throughout the galaxy is homogeneous, being half-solar.

4.10. NGC 7351

A lenticular dwarf galaxy with a low velocity dispersion of stars both in the center and in the disc, and with a low rotation velocity. Its kinematics was previously investigated in [47]. In relation with the low

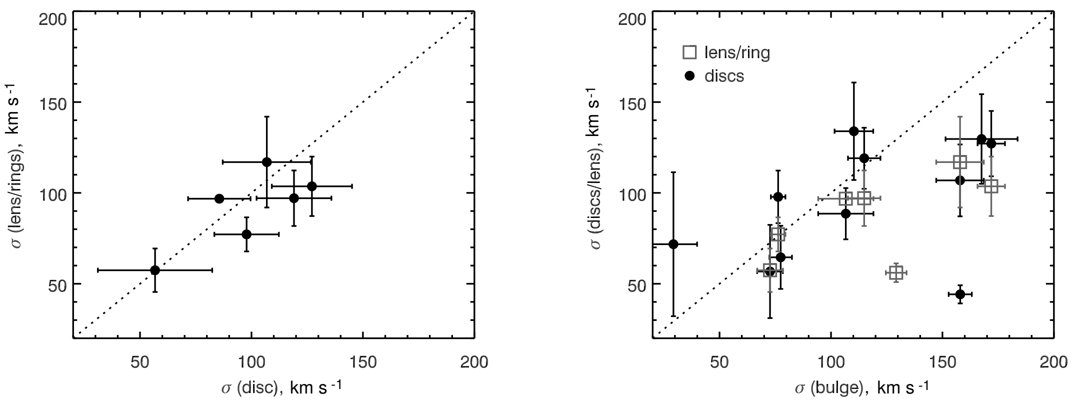

Fig. 4. Left: a comparison of the stellar velocity dispersion in the disc and in separate structures—rings or lenses. Right: a comparison of the stellar velocity dispersion in the bulge and in the disc structures.

luminosity of the galaxy, the metallicity of its stars is below solar, but if in the center it is lower than solar by a factor of 2.5, it is 4 times lower in the disc. The age of the stellar population monotonically increases from the center to the edge of the galaxy, from 1.5 Gyr in the nucleus to 5–8 Gyr in the disc. A comparison with the features of the gaseous component of the galaxy we studied in [21] has shown that in the center the gas rotates with the stars and is excited by the current star formation, and outside the central region the gas exits from the plane of the galactic disc, and its kinematics gets sharply mismatched with the stellar kinematics. In this case accretion of external gas has obviously taken place from a highly inclined orbit, while the stationary conditions for star formation (rejuvenation) have emerged only in the center of the galaxy, where the gas has accumulated and consolidated.

4.11. UGC 4551

Another galaxy with a counter-rotating gas component, which may rotate in the opposite direction to stars right in the plane of the galactic disc [21]. Nevertheless, both the center of the galaxy and its external disc contain a uniformly old, $T > 10$ Gyr, stellar population (Fig. 1). A lens with a flat brightness profile is observed between the bulge and the disc. Here, in the lens, stellar population is significantly younger than in the disc and bulge. From the dynamic point of view both the lens and the disc look quite "hot," $\sigma > 100\ \mathrm{km\,s^{-1}}$.

4.12. UGC 9519

The galaxy, although having an almost face-on orientation to the line of sight ($i = 23°$, HyperLeda), rotates very rapidly (Fig. 1). We [21] have noted the apparent mismatch of the kinematics of gas and stars in the long-slit observations. The panoramic spectroscopy data of the ATLAS-3D survey [5, 18] rather testifies in favor of the internal polar gas disc in this galaxy. As in the case of NGC 7351, the average age of stars monotonically increases along the radius of the galaxy, from 1.5 Gyr in the nucleus to about 5 Gyr in the disc. The disc, being the oldest component of the galaxy, is also the most dynamically hot, $\sigma \approx 100\ \mathrm{km\,s^{-1}}$. It is also the most metal-poor, about twice poorer than the solar chemical composition. In the center of the galaxy a slightly higher than solar metallicity is observed given the recent additional star formation activity.

5. DISCUSSION

Now we have to compare the stellar population parameters of different components of the galaxies: the ratio of average ages of stellar populations will help build a sequence of basic evolutionary stages in the life of the galaxy, while the magnesium-to-iron abundance ratio will allow to limit the duration of the main events of star formation. The main theoretical paradigm to date, the Lambda-CDM model of the evolution of the Universe, predicts that the classical bulges of the early-type disc galaxies are the first ones to get formed in the major merging events, and only then the large-scale discs have to be assembled around them by a smooth accretion of cold gas. However, there are observational facts contradicting these predictions: one after another, the surveys on surface photometry of galaxies consistently demonstrate a correlation between the characteristic sizes of bulges and discs. Interestingly, the presence of this correlation does not depend on whether the given samples of galaxies are dominated by the classical or pseudo-bulges [2, 48, 49]. Thus, it seems like the formation of bulge and disc structures in galaxies is synchronized.

This is exactly what we can see in Fig. 2. A comparison of the average ages of stellar populations of the bulges and flat components, namely, the discs and lenses, shows that our objects are grouped to the bisector, i.e., on the average the ages of the stellar population in the bulge and disc are the same. However, there are two objects in which the age of the disc is confidently shorter than the age of the bulge. This is the essential difference between the properties of the evolution of our *isolated* lenticular galaxies: on the same diagram for the galaxies in denser environments, built by Sil'chenko et al. [50], the objects are grouped in the left upper corner, above the bisector, i.e., the ages of discs are either equal or older compared with the bulge age. It was quite natural to expect this physical difference between the galaxies in groups and isolated galaxies: all the mechanisms of the external effects on the galaxy associated with a dense environment, both gravitational and gas-dynamic, lead to the "inflow" of gas to the galactic center, thus provoking the secondary star formation bursts exactly in the central areas, in the regions dominated by the bulge [51, 52]. Interestingly, the bulges and discs prove to possess equal magnesium-to-iron relations. This means that either the star formation ends quickly in both structures or that it goes on for billions of years here and there. This result, namely, the equality of both the average ages, and the Mg/Fe ratio allows us to strengthen the thesis of the synchronous formation of bulges and discs: the star formation in both starts and ends quasi-simultaneously. At that, the average metallicity of stars in the discs is lower than that in the bulges. Does this mean that the accretion of metal-poor gas mainly occurs in the disc, and the "fuel" for star formation in the bulge gets there after its enrichment by the heavy elements in the disc?

Figure 3 compares the Mg/Fe ratio, characterizing the duration of the last star formation episode, with the other characteristics of stellar population for all three types of structural components. Again, we see an impressive synchronicity of the evolution of bulges and discs: in all the dependencies the points for different structural components are uniformly mixed in the graphs. The correlation of the magnesium-to-iron ratio with the stellar velocity dispersion, characterizing the local density of gravitating mass, is well known for the elliptical galaxies and bulges [53] and is considered to be the proof of the relationship between the star formation efficiency and the potential well depth. However, the left panel of Fig. 3 reveals us for the first time that this correlation is also true for the discs of isolated galaxies, and it is very nearly better than the one for the bulges. By analogy, it can be assumed that the deeper is the local potential well in the galactic plane, the higher is the accretion rate of the external gas, while a higher accretion rate provides for a more efficient star formation.The middle panel of Fig. 3 compares the Mg/Fe ratio and age of the stellar system. We can see the linear envelope on the right (the dotted line), which focuses most of our galaxies. These are probably the stellar systems that have begun their formation in the early Universe at the same time, at $z = 2$–3, and have finished it differently: those that finished it quickly have a high average age of the stellar population and a high Mg/Fe ratio, and those where the star formation continued for many billions of years have evolved to the solar Mg/Fe ratio. However, the distribution in the middle panel of Fig. 3 has a diffuse tail to the left of the dotted line of the main sequence, and this tail contains both discs and bulges. These are the stellar systems where the last star formation episode took place *later* than in the general population of galaxies. Indeed, in order to have both [Mg/Fe]$= +0.2$ and the average stellar population age of 1.5–3 Gyr, they needed to undergo their 1.0–1.5 Gyr of active star formation much later than at $z = 0.5$ redshift. Therefore, it turns out that the star formation episodes in isolated lenticular galaxies may take place at different times and have different durations.

And finally, a few words about the lenses in the S0 galaxies, which are considered to be genetically related with the former rings of star formation. Until now, the prevailing point of view was that the stellar population in lenses is old, and they are dynamically hot [54, 55]. However, this view is based on the study of unitary objects. In our small sample we were able to determine the properties of the stellar population in seven lenses/rings. We can confidently state that the lenses we have studied represent disc structures. On average, they have the same velocity dispersions as those in the discs (the left panel of Fig. 4). When we look at the velocity dispersion profiles, local peaks can be found in the regions of the photometric profile dominated by the lens, for instance, in NGC 3098, NGC 6798, and UGC 4551; however, when performing the averaging across the entire region of the lens, the peaks do not substantially contribute to the resulting averaged velocity dispersion, while by the magnitude the peaks do not differ by more than 20–30 km s^{-1} from the velocity dispersion in the disc which is comparable to the typical velocity dispersion measurement error. The characteristics of the stellar population in the lenses/rings are generally the same as in the discs. We have only found one lens, located in UGC 4551, which is considerably younger than the surrounding disc. At the same time the lenses of an intermediate age, 3–5 Gyr, that agree by their stellar population parameters with the discs were found in five galaxies. With regard to the dynamic status of the bulges, our small sample of isolated lenticular galaxies proved to have practically the same number of pseudo-bulges possessing the same stellar velocity dispersion with their discs, and classical bulges which are dynamically hot (the right panel in Fig. 4). This once again confirms that the bulges in lenticular galaxies can be very different—both by their luminosity and the contribution to the total mass of the galaxy and by their origin and evolution. And this thesis is valid even if we consider a sample of *isolated* lenticular galaxies, in which the influence of the environment on the evolution seems to be minimized.

The results obtained for the stellar components of the sample of isolated lenticular galaxies presented in this article have confirmed our longstanding suspicions about the influence of the environment's density on the evolution of galaxies. Namely, in isolated lenticular galaxies, unlike what is observed in the members of groups and clusters, there is no fixed epoch when the structural components form, they may be generated at a $z > 2$ redshift as well as only a billion years ago. The scatter of average ages in the discs of S0 galaxies indeed increases with decreasing density of the environment of galaxies [50] and reaches its maximum among the isolated galaxies.

On what may the morphological "fate" of a given disc galaxy residing in rarefied surroundings depend? Why can it prove to be lenticular or spiral in our epoch? Everything comes to the mode of accretion of the cold external gas, which usually fuels star formation in the discs of spiral galaxies over billions of years, and this mode is likely to be stochastic. A recent study on finding the faint companions of isolated galaxies [56] has revealed an intriguing statistical feature: in isolated lenticular galaxies the companions have a systematically larger radial velocity difference with the host galaxy than the isolated spiral galaxies, while the isolated lenticular galaxies have no companions whatsoever with the radial velocity difference of less than 50 km s^{-1}. Does this dynamic feature mean that the companions of lenticular galaxies *cannot* infall on their hosts in the near future, whereas for the companions of spiral galaxies the dynamical friction is enough to achieve their timely accretion? Let us reverse the thesis: it is possible that the orbital structure of the group of faint companions is stochastic, and those disc galaxies in which the system of the companions is dynamically cold can provide fuel for the star formation in the disc and become spiral, but those which happened to have a dynamically hot system of companions (or they have already long "dropped" onto themselves all the companions that could be dropped) stay lenticular. A similar hint has appeared in the analysis of rotation of gas systems in the disc galaxies. In virtually all the isolated lenticular galaxies containing gas, its rotation is mismatched with the rotation of stars [21]. This means that the gas was accreted from the orbits inclined to the plane of the main stellar disc, while in the spiral galaxies the gas with the "decoupled" kinematics is much more rare. This might imply that a steady accretion mode in the disc plane provides stable accumulation of the cold gas suitable for continuous star formation, while at the inclined mode of gas infall certain dynamic effects leading to its turbulence and preventing the star formation can occur. For instance, generation of shock waves during the passage of the potential well of the galactic disc [57] or in the collision of the external gas with the primary gas of the galaxy, already existing in the disc. This effect, stemming from the geometry of accretion of the external gas may also affect the formation of the morphological type of a given galaxy.

6. CONCLUSIONS

In this paper we have presented the results of spectroscopic observations of a sample of isolated lenticular galaxies. As a result of observations at the SCORPIO-2 and SCORPIO spectrographs of the 6-meter BTA telescope of the SAO RAS in the long slit mode, we have measured radial profiles of the rotation velocity, velocity dispersion, the average age, and the average metallicity of stars in 12 objects. One of them, IC 875, proved to be a low-luminosity elliptical galaxy; we have analyzed the statistics of the obtained characteristics of the stellar population based on the data of the remaining 11 galaxies. The average ages of the stellar population in our sample of isolated lenticular galaxies fill the full range of values from 1.5 to 15 billion years, and, unlike the S0 galaxies in denser environments, isolated galaxies tend to have the same ages of stars in the bulges and discs, i.e., they do not have the capability of separate bulge rejuvenation. The lenses and rings of increased stellar brightness, detected in 7 of 11 galaxies, usually have stellar populations and stellar velocity dispersion indistinguishable from the stellar populations of the discs. We have concluded that probably the formation of the morphological type of lenticular galaxies in complete isolation critically depends on the possible modes of accretion of external cold gas.

ACKNOWLEDGMENTS

The authors express their gratitude to Dmitry Makarov for his help with the database of galaxies of the Local Volume and construction of the sample of isolated lenticular galaxies, and Nikolay Borisov for his support with the SCORPIO-2 observations at the BTA. In the analysis of the sample galaxies we have used the Lyon–Meudon extragalactic database (HyperLeda), supported by the LEDA team at the Lyon Observatory CRAL (France), and the database of extragalactic data NASA/IPAC (NED), managed by the the Jet Propulsion Laboratory of the California Institute of Technology under a contract with National Aeronautics and Space Administration (NASA, USA). As a source of photometric data, we have used the public archives of the SDSS-III project (`http://www.sdss3.org`), supported by the Alfred P. Sloan foundation, the institutions participating in the SDSS collaboration, the National Science Foundation (NSF), and the U.S. Department of Energy, as well as the data of the Two Micron All Sky Survey (2MASS), which was jointly performed by the University of Massachusetts and the infrared data analysis center at Caltech with the financial support from the NASA and NSF. Our study of isolated lenticular galaxies was supported by the RFBR grants No. 13-02-00059a and 12-02-00685a. I. Katkov expresses gratitude to the nonprofit *Dynasty* foundation for supporting his research. The observations on the 6-meter BTA telescope were held with the financial support of the Ministry of Education and Science of the Russian Federation (state contracts No. 14.518.11.7070, 16.518.11.7073).

REFERENCES

1. E. P. Hubble, *Realm of the Nebulae* (1936).
2. E. Laurikainen, H. Salo, R. Buta, et al., Monthly Notices Royal Astronom. Soc. **405**, 1089 (2010).
3. S. van den Bergh, Astrophys. J. **206**, 883 (1976).
4. J. Kormendy and R. Bender, Astrophys. J. Suppl. **198**, 2 (2012).
5. M. Cappellari, E. Emsellem, D. Krajnović, et al., Monthly Notices Royal Astronom. Soc. **416**, 1680 (2011).
6. L. Spitzer Jr. and W. Baade, Astrophys. J. **113**, 413 (1951).
7. V. Icke, Astronom. and Astrophys. **144**, 115 (1985).
8. G. Byrd and M. Valtonen, Astrophys. J. **350**, 89 (1990).
9. B. Moore, N. Katz, G. Lake, et al., Nature **379**, 613 (1996).
10. J. E. Gunn and J. R. Gott III, Astrophys. J. **176**, 1 (1972).
11. V. Quilis, B. Moore, and R. Bower, Science **288**, 1617 (2000).
12. R. B. Larson, B. M. Tinsley, and C. N. Caldwell, Astrophys. J. **237**, 692 (1980).
13. A. Dressler, Astrophys. J. **236**, 351 (1980).
14. A. Naim, O. Lahav, R. J. Buta, et al., Monthly Notices Royal Astronom. Soc. **274**, 1107 (1995).
15. J. W. Sulentic, L. Verdes-Montenegro, G. Bergond, et al., Astronom. and Astrophys. **449**, 937 (2006).
16. O. K. Sil'chenko, I. V. Chilingarian, N. Y. Sotnikova, and V. L. Afanasiev, Monthly Notices Royal Astronom. Soc. **414**, 3645 (2011).
17. A. V. Zasov, O. K. Sil'chenko, I. Y. Katkov, and S. N. Dodonov, Astronomy Letters **39**, 17 (2013).
18. T. A. Davis, K. Alatalo, M. Sarzi, et al., Monthly Notices Royal Astronom. Soc. **417**, 882 (2011).
19. Y. Birnboim, A. Dekel, and E. Neistein, Monthly Notices Royal Astronom. Soc. **380**, 339 (2007).
20. R. Sancisi, F. Fraternali, T. Oosterloo, and T. van der Hulst, Astronom. Astrophys. Rev. **15**, 189 (2008).
21. I. Y. Katkov, O. K. Sil'chenko, and V. L. Afanasiev, Monthly Notices Royal Astronom. Soc. **438**, 2798 (2014).
22. I. D. Karachentsev and D. I. Makarov, Astrophysical Bulletin **63**, 299 (2008).
23. D. I. Makarov and I. D. Karachentsev, Astrophysical Bulletin **64**, 24 (2009).
24. D. Makarov and I. Karachentsev, Monthly Notices Royal Astronom. Soc. **412**, 2498 (2011).
25. I. D. Karachentsev, D. I. Makarov, V. E. Karachentseva, and O. V. Melnyk, Astrophysical Bulletin **66**, 1 (2011).
26. V. L. Afanasiev and A. V. Moiseev, Baltic Astronomy **20**, 363 (2011).
27. V. L. Afanasiev and A. V. Moiseev, Astronomy Letters **31**, 194 (2005).
28. P. G. van Dokkum, Publ. Astronom. Soc. Pacific **113**, 1420 (2001).
29. I. Y. Katkov and I. V. Chilingarian, ASP Conf. Ser., No. 442, 143 (2011).
30. P. Prugniel, C. Soubiran, M. Koleva, and D. Le Borgne, arXiv:astro-ph/0703658 (2007).
31. M. Cappellari and E. Emsellem, Publ. Astronom. Soc. Pacific **116**, 138 (2004).
32. R. P. van der Marel and M. Franx, Astrophys. J. **407**, 525 (1993).
33. I. Chilingarian, P. Prugniel, O. Sil'chenko, and M. Koleva, IAU Symp., No. 241, 175 (2007).
34. I. V. Chilingarian, P. Prugniel, O. K. Sil'chenko, and V. L. Afanasiev, Monthly Notices Royal Astronom. Soc. **376**, 1033 (2007).
35. D. Le Borgne, B. Rocca-Volmerange, P. Prugniel, et al., Astronom. and Astrophys. **425**, 881 (2004).
36. E. E. Salpeter, Astrophys. J. **121**, 161 (1955).
37. C. J. Walcher, P. Coelho, A. Gallazzi, and S. Charlot, Monthly Notices Royal Astronom. Soc. **398**, L44 (2009).
38. P. Prugniel and M. Koleva, IAU Symp., No. 284, 16 (2012).
39. B. M. Tinsley, Astrophys. J. **229**, 1046 (1979).
40. F. Matteucci and L. Greggio, Astronom. and Astrophys. **154**, 279 (1986).
41. G. Worthey, S. M. Faber, J. J. Gonzalez, and D. Burstein, Astrophys. J. Suppl. **94**, 687 (1994).
42. L. A. Jones and G. Worthey, Astrophys. J. Letters **446**, L31 (1995).
43. D. Thomas, C. Maraston, and R. Bender, Monthly Notices Royal Astronom. Soc. **339**, 897 (2003).

44. R. L. Davies, G. Efstathiou, S. M. Fall, et al., Astrophys. J. **266**, 41 (1983).
45. S. Barway, Y. D. Mayya, A. K. Kembhavi, and S. K. Pandey, Astronom. J. **129**, 630 (2005).
46. W. Seifert and C. Scorza, Astronom. and Astrophys. **310**, 75 (1996).
47. F. Simien and P. Prugniel, Astronom. and Astrophys. **384**, 371 (2002).
48. L. A. MacArthur, S. Courteau, and J. A. Holtzman, Astrophys. J. **582**, 689 (2003).
49. J. Méndez-Abreu, J. A. L. Aguerri, E. M. Corsini, and E. Simonneau, Astronom. and Astrophys. **478**, 353 (2008).
50. O. K. Sil'chenko, I. S. Proshina, A. P. Shulga, and S. E. Koposov, Monthly Notices Royal Astronom. Soc. **427**, 790 (2012).
51. K. Bekki and W. J. Couch, Monthly Notices Royal Astronom. Soc. **415**, 1783 (2011).
52. T. Kronberger, W. Kapferer, C. Ferrari, et al., Astronom. and Astrophys. **481**, 337 (2008).
53. S. C. Trager, S. M. Faber, G. Worthey, and J. J. González, Astronom. J. **120**, 165 (2000).
54. J. Kormendy, Astrophys. J. **286**, 116 (1984).
55. E. Laurikainen, H. Salo, E. Athanassoula, et al., Monthly Notices Royal Astronom. Soc. **430**, 3489 (2013).
56. V. E. Karachentseva, I. D. Karachentsev, and O. V. Melnyk, Astrophysical Bulletin **66**, 389 (2011).
57. K.-I. Wakamatsu, Astronom. J. **105**, 1745 (1993).

Translated by A. Zyazeva